Discrete Willmore Flow

Alexander I. Bobenko[1] and Peter Schröder[2]

[1]TU Berlin [2]Caltech

Abstract

The Willmore energy of a surface, $\int (H^2 - K)\,dA$, as a function of mean and Gaussian curvature, captures the deviation of a surface from (local) sphericity. As such this energy and its associated gradient flow play an important role in digital geometry processing, geometric modeling, and physical simulation. In this paper we consider a discrete *Willmore energy and its flow. In contrast to traditional approaches it is not based on a finite element discretization, but rather on an ab initio discrete formulation which preserves the Möbius symmetries of the underlying continuous theory in the discrete setting. We derive the relevant gradient expressions including a linearization (approximation of the Hessian), which are required for non-linear numerical solvers. As examples we demonstrate the utility of our approach for surface restoration, n-sided hole filling, and non-shrinking surface smoothing.*

Categories and Subject Descriptors (according to ACM CCS): G.1.8 [Numerical Analysis]: Partial Differential Equations; I.3.5 [Computer Graphics]: Computational Geometry and Object Modeling; I.6.8 [Simulation and Modeling]: Types of Simulation.

Keywords: Geometric Flow; Discrete Differential Geometry; Willmore Energy; Variational Surface Modeling; Digital Geometry Processing.

1. Introduction

The *Willmore* energy of a surface $S \subset \mathbb{R}^3$ is given as

$$E_W(S) = \int_S (H^2 - K)\,dA = 1/4 \int_S (\kappa_1 - \kappa_2)^2\,dA,$$

where κ_1 and κ_2 denote the principal curvatures, $H = 1/2(\kappa_1 + \kappa_2)$ and $K = \kappa_1 \kappa_2$ the mean and Gaussian curvature respectively, and dA the surface area element. Immersions of surfaces which minimize this energy are of great interest in several areas:

- **Theory of surfaces**: the Willmore energy of a surface is conformally invariant [Bla29] making it an important functional in the study of conformal geometry [Wil00];

- **Geometric modeling**: for compact surfaces with fixed boundary a minimizer of $E_W(S)$ is also a minimizer of total curvature $\int_S \kappa_1{}^2 + \kappa_2{}^2\,dA$ which is a standard functional in variationally optimal surface modeling [LP88, WW94, Gre94];

- **Physical modeling**: thin flexible structures are governed

by a surface energy of the form

$$E(S) = \int_S \alpha + \beta (H - H_0)^2 - \gamma K\,dA,$$

the so-called Canham-Helfrich model [Can70, Hel73] (H_0 denotes the "spontaneous" curvature which plays an important role in thin-shells [GKS02, BMF03, GHDS03]). For $\alpha = H_0 = 0$, $\beta = \gamma$ the Canham-Helfrich model reduces to the Willmore energy.

In all of these application areas one typically deals with the associated geometric flow

$$\dot{S} = -\nabla E(S),$$

(time derivatives are denoted by an overdot) which drives the surface to a minimum of the potential energy given by $E(S)$. In the theory of surfaces as well as in geometric modeling one is interested in critical points of $E(S)$. In physical modeling the solution shape is characterized by a balance of external and internal forces. In this setting the internal forces are a function of the Willmore gradient.

Contributions In this paper we explore a novel, discrete Willmore energy [Bob05] and introduce the associated *geometric flow* for piecewise linear, simplicial, 2-manifold meshes. In contrast to earlier approaches the discrete flow is not defined through assemblies of lower level discrete operators, nor does the numerical treatment employ operator splitting approaches. Instead the discrete Willmore energy, defined as a function of the vertices of a triangle mesh, is used directly in a non-linear numerical solver to affect the associated flow as well as solve the static problem. Since the discrete formulation has the same symmetries as the continuous problem, *i.e.*, it is Möbius invariant, the associated properties, such as invariance under scaling, carry over *exactly* to the discrete setting of meshes. To deal effectively with boundaries we introduce appropriate boundary conditions. These include position and tangency constraints as well as a free boundary condition. We demonstrate the method with some examples from digital geometry processing and geometric modeling.

1.1. Related Work

We distinguish here between *discrete* geometric flows, *i.e.*, flows based on discrete analogues of continuous differential geometry quantities, and those based on *discretizations* of continuous systems. The guiding principle in the construction of the former is the preservation of symmetries of the original continuous system, while the latter is based on traditional finite element or finite difference approaches which in general do not preserve the underlying symmetries. There is also a broad body of literature which uses linearized versions of the typically non-linear geometric functionals. Such approaches are not based on intrinsic geometric properties (*e.g.*, replacing curvatures with second derivatives) but rather depend on the particular parameterization chosen. For this reason we will not further consider them here.

Discrete Flows In the context of mesh based geometric modeling a number of discrete flows have been considered. For example, Desbrun *et al.* [DMSB99] used mean curvature flow ($\alpha = 1$, $\beta = \gamma = H_0 = 0$) to achieve denoising of geometry. Pinkall and Polthier [PP93] used a related approach, area minimizing flow, to construct discrete minimal surfaces. Critical points of the area functional also play an important role in the construction of discrete harmonic functions [DCDS97], their use in parameterizations [EDD*95, DMA02], and the construction of conformal structures for discrete surfaces [Mer01, GY03]. Since the underlying "membrane" energy is second order only, it cannot accomodate G^1 continuity conditions at the boundary of the domain. These are important in geometric modeling for the construction of tangent plane continuous surfaces. Fourth order flows on the other hand can accomodate position and tangency conditions at the boundary. Perhaps the simplest fourth order flow is *surface diffusion*, *i.e.*, flow by the Laplace-Beltrami operator of mean curvature, $\dot{S} = -\Delta_S H$. Such discrete flows were studied by Schneider

and Kobbelt [SK01], Xu *et al.* [XPB05], and Yoshizawa and Belyaev [YB02]. In each case the approach was based on taking the square of a discrete Laplace-Beltrami operator combined with additional simplifications to ease implementation. Unfortunately surface diffusion flow can lead to singularities in finite time [MS00] leading to "pinching off" of surfaces which are too thin. Yoshizawa and Belyaev [YB02] demonstrate this behavior and show the comparison with Willmore flow, which leads to much better results in this regard. This difference in behavior between surface diffusion and Willmore flows is due to the additional terms appearing in the Euler-Lagrange (EL) equation of the Willmore flow

$$\Delta_S H + 2H(H^2 - K) = 0.$$

Yoshizawa and Belyaev took the EL equation as their starting point and defined a discrete Willmore flow by assemblying the components from individual, well known discrete operators. Unfortunately in that discrete setting properties such as $H^2 - K \geq 0$ can no longer be guaranteed. In contrast we define our discrete Willmore energy directly using the Möbius invariance of the integrand $(H^2 - K)\,dA$ as the fundamental principle. Among other properties one achieves the $H^2 - K \geq 0$ always, as expected (see Section 2).

Discretized Flows Both surface diffusion and Willmore flows have been treated numerically through a variety of discretizations. For example, Tasdizen *et al.* [TWBO03] and Chopp and Sethian [CS99] use a level set formulation for surface diffusion flow, while Mayer [May01] uses finite differences, and Deckelnick *et al.* [DDE03] use finite elements. For Willmore flow finite element approaches were pursued by Hari *et al.* [HGR01] and Clarenz *et al.* [CDD*04]. A level set formulation was given by Droske and Rumpf [DR04]. In these approaches no attempt is made to preserve the Möbius symmetries. On the other hand they do have the advantage that a rich body of literature applies when it comes to error and convergence analysis. Our approach as of now lacks a complete analysis of this type. Partial results on the convergence of the discrete Willmore energy to the continuous Willmore energy are discussed at the end of Section 2.

2. Discrete Willmore Energy

In this section we recall the definition of the discrete Willmore energy and some of its relevant properties.

The derivation of the discrete Willmore energy is based on the observation that the integrand

$$(H^2 - K)\,dA$$

is invariant under Möbius transformations [Bla29], *i.e.*, translations, rotations, uniform scale, and inversion. The first two are obvious and the latter two follow from the change of variable formula [Che73]. This immediately implies that $E_W(S)$ itself is a conformal invariant of the surface. Note that for compact closed surfaces we also have $E_H(S) = \int_S H^2\,dA$ as a conformal invariant [Whi73]. However the *integrand* of

$E_H(S)$ is *not* Möbius invariant. It is for this reason that we prefer E_W over E_H (the latter is used by some authors as the definition of the Willmore energy).

The Möbius invariance is a natural mathematical discretization principle. The importance of this property depends on the particular application one is interested in. For the numerical construction of Willmore surfaces, which are critical points (in particular minima) of the Willmore energy, it is essential. For applications such as smoothing and denoising of meshes (see Section 4) a concrete benefit is the scale invariance of the Willmore energy.

We are interested in evaluating this energy for discrete surfaces, *i.e.*, surfaces given as topological 2-manifold configurations of simplicies. Such a "mesh" consists of vertices $v_i = (x_i, y_i, z_i)^T$ $(i = 1, \ldots, N)$ and the topological complex is given as a set of edges e_{ij} connecting v_i with v_j and triangles t_{ijl} bounded by vertices v_i, v_j and v_l and edges e_{ij}, e_{jl}, and e_{li} (see Figure 1). For notational simplicity we assume that the surface is closed (*i.e.*, each edge e_{ij} is bounded by exactly two triangles, t_{ijl} and t_{jik}) and that triangles incident on a given edge are consistently oriented (note however that we do not assume global orientability). Boundaries will be discussed in Section 3.3.
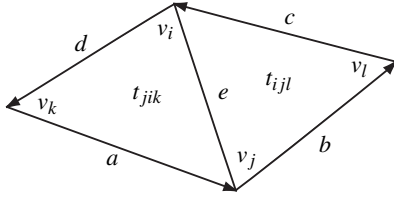

Figure 1: *Notation for vertices, edges and triangles in the vicinity of a given edge $e = (v_i, v_j) = e_{ij}$; $a = e_{kj}$, $b = e_{jl}$, $c = e_{li}$, $d = e_{ik}$.*

The discrete Willmore energy on a mesh is defined at each vertex v_i as

$$W_i = \sum_{e_{ij}} \beta_j^i - 2\pi,$$

i.e., a sum over the edges incident to v_i of certain angles β_j^i, which measure the angle between the circumcircles defined by the two triangles t_{ijl} and t_{jik} incident to the given edge e_{ij} (see Figure 2). Obviously W_i is Möbius invariant since its definition is based on angles between circles. The Willmore energy of the entire mesh is then simply the sum, $W = \sum_i W_i$. For later use we also recall the definition of discrete Gauss curvature at a vertex v_i

$$K_i = 2\pi - \sum_{t_{ikj}} \alpha_{kj}^i.$$

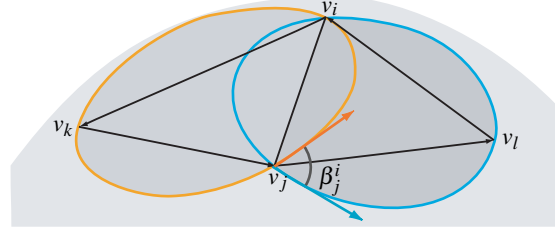Here α_{kj}^i denotes the Euclidean angle at i inside the triangle t_{ikj}.

Figure 2: *Geometry of β_j^i.*

The geometric picture is as follows. A given edge has two incident triangles. Each triangle has a circumcircle. Since the four vertices forming the two triangles are (generically) on a common sphere (possibly at infinity) the two circumcircles are also on this sphere. The two circles meet in the vertices v_i and v_j where they intersect. Consider a tangent vector to each circle at v_i. These two tangent vectors make the angle β_j^i which lies in the tangent plane to the sphere at that point. Note that this geometric setup implies that $\beta_j^i = \beta_i^j$. Suppose now v_i and all its neighbors v_j (*i.e.*, corresponding to edges e_{ij}) lie on a common sphere and that the (embedded) 1-ring of v_i is convex. In that case it is easy to see that the β_j^i neatly add up to exactly 2π in the tangent plane at v_i and hence $W_i = 0$ (see Figure 3) as expected. Now suppose that v_i and its neighboring vertices do not share a common sphere. In that case $W_i > 0$. To see this use the Möbius invariance of the energy and map the central point v_i to infinity by a Möbius transformation. All circles passing through v_i are mapped to straight lines and the energy becomes the sum $\sum_j \beta_j^i$ of the external angles of a non-planar closed polygon in three space. In that interpretation the inequality $\sum_j \beta_j^i \geq 2\pi$ follows easily [Bob05] (this inequality is a polygonal version of Fenchel's theorem [Fen29, Spi75]). With the same argument one also concludes that $W_i + K_i \geq 0$, *i.e.*, $\sum_j \beta_j^i - \sum_{kj} \alpha_{kj}^i \geq 0$, reflecting the fact that $H^2 dA$ is always non-negative.

Finally we observe that $W_i \geq 0$ and that it vanishes iff v_i and all its edge neighbors v_j lie on a common sphere and the vertex v_i is convex. These two conditions are equivalent to the condition that the triangles meeting at v_i build a Delaunay triangulation on a sphere.

Smooth Limit The discrete Willmore energy W is not only an analogue of the continuous one. It approximates the continuous Willmore energy $\mathcal{W}$ in a "natural" limit. Let $(u, v) \mapsto f(u, v)$ be a curvature line parameterization of a surface. Without loss of generality consider the vicinity of the origin $(u, v) = (0, 0)$ in the tangent plane where we have

$$(u, v) \mapsto \left(u, v, \frac{1}{2}(\kappa_1 u^2 + \kappa_2 v^2) + o(u^2 + v^2)\right),$$

with κ_1, κ_2 denoting the principal curvatures of the surface at the point $(0, 0)$. Now consider a triangular lattice $L_\varepsilon = \{\varepsilon(la + mb + nc) : l, m, n \in \mathbb{Z}\}$ in the parameter plane generated by three vectors a, b, c with $a + b + c = 0$. Here ε is a small parameter. Consider the hexagon D_ε in the parameter
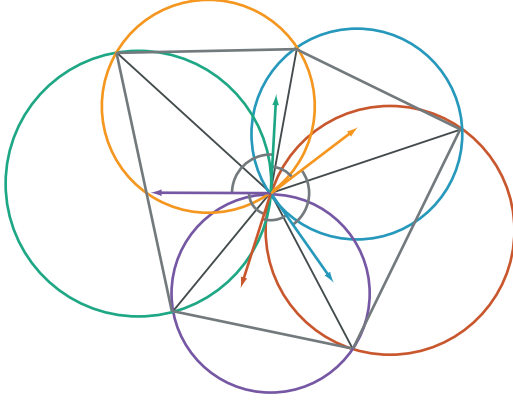
Figure 3: *Geometry of $\sum_{e_{ij}} \beta_j^i$ around a vertex. The angles between subsequent circumcircles—appropriate tangent vectors are indicated with colors corresponding to the circumcircles of each triangle—neatly add up to 2π if all vertices are co-spherical.*

plane with vertices $p_1 = \varepsilon a$, $p_2 = -\varepsilon c$, $p_3 = \varepsilon b$, $p_4 = -\varepsilon a$, $p_5 = \varepsilon c$, $p_6 = -\varepsilon b$ and its image $f(D_\varepsilon)$ on the surface. Let $\mathscr{W}(D_\varepsilon)$ be the smooth Willmore energy of $f(D_\varepsilon)$. On the other hand, the vertices $f(p_i)$, $i = 1,\ldots,6$ together with $f(0)$ build a simplicial surface with six triangles. Denote by $W(D_\varepsilon)$ the discrete Willmore energy of this surface and consider the quotient of the discrete and smooth Willmore energies of such an infinitesimal hexagon

$$R = \lim_{\varepsilon \to 0} \frac{W(D_\varepsilon)}{\mathscr{W}(D_\varepsilon)}.$$

A direct but rather complicated computation leads to the following conclusions:

1. R is independent of the curvatures κ_1, κ_2,

2. $R \geq 1$, and $R = 1$ iff the lattice L_ε has two of its directions aligned with the curvature lines of the surface (two of the vectors a, b, c are curvature line directions).

Thus, after sufficiently many $1 \to 4$ refinements of the smooth surface the discrete Willmore energy approximates the smooth one if the curvature line net is triangulated, otherwise the discrete energy is larger.

The question whether the discrete Willmore energy can be used as a variational method for computation of curvature line nets is currently under investigation (see also Figures 8 and 9).

3. Evaluation

For the numerical treatment of discrete Willmore flow and the solution of energy minimization problems we need effective evaluation procedures for the Willmore energy and its derivatives. To simplify the implementation of these functions we begin with a discussion of the definition of the angles β_j^i and some of the consequent symmetries in the expressions.

3.1. Definition of Intersection Angles

Consider edge e_{ij} and its two incident triangles t_{jik} and t_{ijl} with associated vertices v_k, v_j, v_l, and v_i (see Figure 1). Defining the four directed edge vectors

$$A = \frac{a}{|a|} = \frac{v_j - v_k}{|v_j - v_k|} \quad B = \frac{b}{|b|} = \frac{v_l - v_j}{|v_l - v_j|}$$

$$C = \frac{c}{|c|} = \frac{v_i - v_l}{|v_i - v_l|} \quad D = \frac{d}{|d|} = \frac{v_k - v_i}{|v_k - v_i|}$$

the angles follow as

$$\cos \beta_j^i = -R(Q) = -R(AB^{-1}CD^{-1})$$
$$= \langle A,C \rangle \langle B,D \rangle - \langle A,B \rangle \langle C,D \rangle - \langle B,C \rangle \langle D,A \rangle,$$

where $\langle .,. \rangle$ denotes the usual Euclidean dot product and $R(Q)$ the real part of the normalized cross ratio of the four edges bounding the "diamond" formed by the two triangles incident on edge e_{ij}. This cross ratio is defined in terms of quaternion algebra with the standard identification of 3-vectors with imaginary quaternions, $\mathbb{R}^3 \equiv I(\mathbb{H})$, $v \mapsto (0, ix, jy, kz)^T$ ($i^2 = j^2 = k^2 = -1$, $ij = k$, $jk = i$, $ki = j$). The subsequent expression of this quaternion cross ratio in terms of Euclidean inner products follows from the rules of quaternion multiplication and Lagrange's identity for the inner product between two cross products. More details can be found in [Bob05].

Properties of β_j^i and its Derivatives A number of surprising facts—which we exploit to significantly simplify the expressions needed by the numerical solver—are immediately obvious from the above definition. To clarify these we make all arguments explicit, $\beta_j^i = \beta(k,j,l,i)$ going around the diamond in counter clockwise order. We already noted earlier that $\beta(k,j,l,i) = \beta(l,i,k,j)$. In fact from the formula for $\cos \beta(k,j,l,i)$ it terms of scalar products it is immediately clear that $\beta(k,j,l,i)$ is invariant under all cyclic permutations and reflections of its arguments. In particular if we flip the edge $e_{ij} \mapsto e_{kl}$ the cosine of the angle remains the same.

From the invariance under cyclic and reflection permutations of its arguments it also follows that all first derivatives can be written as a single function $f_1(.,.,.,.)$ with suitably permuted arguments

$$\beta_{,k} = f_1(k,j,l,i) \quad \beta_{,j} = f_1(j,l,i,k)$$
$$\beta_{,l} = f_1(l,i,k,j) \quad \beta_{,i} = f_1(i,k,j,l).$$

(Here and in what follows we use comma notation to denote partial derivatives with respect to the corresponding argument and write $\beta := \beta_j^i$ to reduce clutter.)

3.2. Energy Gradient

For gradient flow numerical computations we require the gradient of the discrete Willmore energy. A direct calcula-

tion readily yields

$$-\sin(\beta)\beta_{,k} = (-\frac{1}{|a|}P_A(C)\langle B,D\rangle + \langle A,C\rangle\frac{1}{|d|}P_D(B)$$
$$+\frac{1}{|a|}P_A(B)\langle C,D\rangle - \langle A,B\rangle\frac{1}{|d|}P_D(C)$$
$$-\langle B,C\rangle(\frac{1}{|d|}P_D(A)-\frac{1}{|a|}P_A(D))).$$

Here we used $P_X = I - X \otimes X$ as shorthand for the projection operator into the orthogonal complement of (the unit vector) X.

Remarkably, if we separate out the linear dependence of this expression on a, b, c, and d we arrive at a *scalar* linear combination

$$-\sin(\beta)\beta_{,k} = (\frac{\cos\beta}{|a|^2}-\frac{\langle B,C\rangle}{|a||d|})a$$
$$+(\frac{\langle A,C\rangle}{|b||d|}+\frac{\langle C,D\rangle}{|b||a|})b$$
$$-(\frac{\langle A,B\rangle}{|c||d|}+\frac{\langle B,D\rangle}{|c||a|})c$$
$$-(\frac{\cos\beta}{|d|^2}-\frac{\langle B,C\rangle}{|a||d|})d. \qquad (1)$$

In a semi-implicit time stepping algorithm this amounts to requiring only the solution of a sparse linear system of size $n \times n$ rather than $(3n) \times (3n)$ for n vertices, a very attractive feature. In fact Equation 1 can serve as a linearized version of the Hessian of the energy. See Section 4 for further comments on this fact.

For the free boundary treatment we also need expressions for the gradient of the angle between two edges. Desbrun and co-workers [DMA02] (Appendix B) derive these and we will not repeat them here.

Gradient Singularity If v_k, v_j, v_l, and v_i are co-circular then $\beta = 0$ and $\beta_{,k}$ is not defined. For vertices in general positions this does not occur. However, in practice the case that the four vertices of a diamond are nearly co-circular, while rare, does occur. For some inputs it can in fact be a frequent occurance (see for example Figure 12). Consider a quadrangulation of a smooth surface which is turned into a triangle mesh through insertion of diagonals in each quad. In this setting the diagonal edges very often have β nearly equal to zero.

Keeping in mind that in the end we care about the direction of *negative gradient*, *i.e.*, steepest descent, of the discrete Willmore energy we make the following geometric observation. In case $\beta = 0$ there is one direction of varying v_k in which the angle does not change (infinitesimally). This is the tangential direction to the circle C passing through the points v_i, v_j, v_k and v_l. For (infinitesimal) unit motions in all orthogonal directions the angle β increases at equal rate. This property of the gradient is conformal and thus preserved under Möbius transformations. It can be seen more easily in a

Möbius transformed picture. Send the point v_i to infinity by the inversion in a sphere centered at v_i. Both circles in Figure 4 become straight lines. Let $\tilde{v}_j, \tilde{v}_k, \tilde{v}_l$ be the images of the vertices v_j, v_k, v_l under this Möbius transformation. For the case of $\beta = 0$ both circles in Figure 4 are coincident—call this common circle C—and the points $\tilde{v}_j, \tilde{v}_k$ and $\tilde{v}_l$ become collinear: they lie on the straight line L which is the Möbius image of the circle C. The only direction of varying $\tilde{v}_k$ in which the angle does not change is along the straight line L. Variations in all orthogonal directions increase the angle at equal rate.
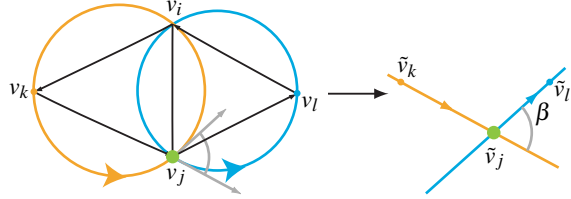

Figure 4: *After sending v_i to infinity, the two circles have been mapped to two lines which intersect with angle β.*

Consider now a given vertex v_i and assume for the moment that only one β contributing to the gradient computation at v_i vanishes. Let $C \ni v_i$ be the corresponding circle with four vertices lying on it. Let all other, well defined, negative gradient directions sum to g. Decompose a variation direction $G = G_o + G_p$ of v_i into the parts orthogonal $G_o \perp C$ and parallel $G_p \parallel C$ to the tangent of the circle in v_i and let $g = g_o + g_p$ be the same decomposition of g. The contribution to the gradient from all "regular" (non-vanishing) β's is $-\langle g, G\rangle$ and the contribution of the vanishing β is $R \mid G_o \mid$ with some $R > 0$. For the whole gradient this implies

$$-G_p g_p + (\mid G_o \mid R - \langle G_o, g_o\rangle).$$

Thus the total negative gradient direction, i.e. the direction in which the energy decreases the most is g_p (parallel to C) if $R > \mid g_o \mid$ and $g_p + g_o(1 - R/\mid g_o \mid)$ if $R < \mid g_o \mid$.

The case of multiple β's in the support of the gradient of W_i with respect to the given vertex v_i vanishing, is more complicated. One can get the negative gradient direction (if it exists) in this case from the following non-linear minimization process. To each of the edges e_n with vanishing $\beta(e_n) = 0$ there corresponds a circle C_n through v_i. For the variation G the contribution to the gradient of this edge is $\mid R_n \times G \mid$ where R_n is a vector tangent to C_n. We define

$$\delta = \min_{|G|=1, \langle G,g\rangle \geq 0} \sum_n |R_n \times G| - \langle G, g\rangle$$

where the sum is taken over all vanishing β from the 1-ring with flaps of v_i. The first term measures the length of the projection of G into the orthogonal complement of R_n, *i.e.*, the amount of (infinitesimal) increase of energy while the second term measures the decrease in energy for the direction G. If $\delta > 0$ no motion exists which decreases the energy and

the direction of steepest descent is the zero vector. If $\delta < 0$ the direction G which achieves the minimum is our sought after steepest descent direction with magnitude $|\delta|$.

The case that all β in the support of the gradient of v_i vanish simultaneously, corresponds to a configuration which puts all vertices in the 1-ring with flaps of v_i including v_i itself onto a common circle. In this case no direction decreasing the Willmore energy at v_i exists.

In our implementation we have experimented with the non-linear minimization to find a valid direction of energy decrease (or zero if none exists) but found it to give the same results (numerically) as a far simpler heuristic: if $|\sin\beta| < \varepsilon$ set the corresponding gradient to zero. We found $\varepsilon = 10^{-6}$ to give reliable results in double precision for all our experiments.

3.3. Boundary Conditions

So far we have implemented two types of boundary conditions.

G^1-**boundary** The variational problem we are dealing with is a fourth order system. To be well posed it requires two independent boundary conditions. The most natural choice here is to fix positions and normals at a boundary. We specify this kind of boundary data on a mesh by fixing positions of the boundary vertices and those vertices within one edge distance from the boundary. The normals of the triangles of this boundary strip can be treated as normals on the boundary. This boundary condition fits perfectly for G^1-gluing of surfaces. Typical applications are surface restoration and smooth filling of a hole (see Figures 10 and 11). Note that the method requires no conditions on the topology of the mesh. In particular one can fix some "islands" of internal vertices (or faces) of the required surface.

Free Boundary Alternatively we have experimented with closing boundary curves by adding a vertex at infinity to each boundary loop. This is an unusual treatment since it actually removes the boundary and adds a Dirichlet condition at infinity. The idea comes from Möbius geometry where the infinity point is not distinguished.
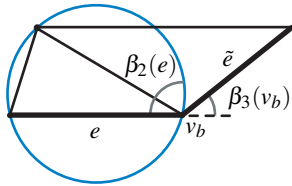

Figure 5: *Free boundary conditions. Boundary edges e and $\tilde{e}$, and a boundary vertex v_b with the angles β_2 and β_3.*

For simplicity consider a surface with one boundary curve.

By adding the infinity point and connecting it to each boundary vertex we obtain a closed surface. We distinguish three types of edges of this surface $E = E_i \cup E_b \cup E_\infty$: internal edges E_i, boundary edges E_b of the original surface and new edges E_∞ incident to the infinity point. The circumcircles passing through the infinity point are straight lines. The discrete Willmore energy of the closed surface consists of three terms

$$\sum_{e \in E} \beta(e) = \sum_{e \in E_i} \beta_1(e) + \sum_{e \in E_b} \beta_2(e) + \sum_{e \in E_\infty} \beta_3(e).$$

The first term is just the discrete Willmore energy of the original surface. The angles $\beta_2(e)$ are associated to the boundary edges $e \in E_b$ and are the intersection angles of these edges with the circumcircles of the corresponding boundary triangles. Another interpretation for $\beta_2(e)$ is that this is π minus the angle of the boundary triangle opposite to the edge $e \in E_b$. Finally the angle $\beta_3(e)$ is associated to the additional edge $e \in E_\infty$ connecting ∞ to a boundary vertex v_b. Equivalently it can be associated to the boundary vertex v_b. This is the intersection angle of two circumcircles (which are straight lines in this case) passing through v_b and ∞, *i.e.*, the intersection angle of two boundary edges meeting at v_b (see Figure 5).

The resulting behavior is that of a free boundary (see Figure 7; right column).

4. Numerical Experiments

We have implemented the discrete Willmore gradient flow using linear and non-linear solvers from the excellent PETSc [BBE*04] and TAO [BMMS04] libraries, allowing us to experiment with a wide variety of pre-canned solvers, while needing to supply only the gradient, respectively the approximation of the Hessian (Equation 1). For the time discretization we experimented with both the forward and backward Euler method. For the forward Euler method the time step limitation imposed by the Courant condition for fourth order problems—time increments must be of the order of the fourth power of the shortest edge in the mesh—is too severe to be practical except for very simple meshes. The backward Euler method leads to a non-linear problem at each step. These can be solved with a full Newton method requiring evaluation of the Hessian of the energy at each iteration step. We did derive the expressions for the Hessian, but found that the effort was not justified as a function of evaluation cost and numerical behavior. The latter was no better in our experiments than a much simpler approach based on a semi-implicit time discretization using the linearized version of the gradient (Equation 1). In that setup only a *linear* system must be solved at each time step to find the position increment $\Delta x^{(t)}$

$$(\frac{1}{dt}\mathbb{I} + K^{(t)})\Delta x^{(t)} = -\nabla E^{(t)}.$$

Here dt is the time step and a super script $^{(t)}$ denotes quantities evaluated at time t. The matrix K is $n \times n$ where n is

the number of (free) vertices and collects the terms of Equation 1. Assuming an average valence of six, each row of the matrix contains (on average) thirteen non-zero entries (1-ring with flaps plus the center vertex). The full Hessian has non-trivial 3×3 blocks instead and results in a linear system of size $(3n) \times (3n)$.

The use of such approximations is well established and works well in practice though the usual convergence guarantees of Newton methods are missing. Desbrun and co-workers [DMSB99] used a similar approach when they performed implicit mean curvature flow with a constant matrix per time step. Recall that the coefficients of the "cotan formula" change throughout the time step. Keeping them constant corresponds to a similar linearization of the gradient as we employed. For the particular case of problems involving squared curvature bending energies Hauth and co-workers [HES03], similarly found that inexact Newton methods using even fairly aggressive linearizations of gradients work very well.

Figures 6 and 7 show some simple examples. The icosahedron is subdivided linearly four times and becomes essentially a perfect sphere within a few minimization steps (Figure 6). After 24 steps convergence was achieved with a final energy of 10^{-7} (a perfect sphere would be zero). The difference between fixed and free boundary conditions is illustrated with the cathead example (Figure 7). First the result of flow with fixed boundaries then the result of keeping the boundaries free (both intermediate and final state shown). The latter evolves to a planar polygon with convex boundaries. In the latter example we show the circumcircles for all triangles.

Figure 8 shows the evolution of a torus. The initial mesh is a coarse torus linearly subdivided twice. Almost immediately the vertices flow to the surface of a geometric torus. Subsequent evolution aligns edges with the principal curvature directions (and "fattens" the torus). The edge alignment also becomes apparent in the flat-shaded highlights. Figure 9 shows a pipe with two boundary loops which are circular (in essence half the torus example with fixed boundaries). The same evolution as with the torus can be observed with the long term behavior evolving towards a "fat" pipe.

Figure 10 shows a standard benchmark example from k-sided (six in this case) hole filling. An initial triangulation with boundaries coming from a Loop subdivision surface is relaxed under the Willmore flow. With the two outermost "rows" of vertices fixed tangent continuity across the boundary is assured. Note that this example starts in a configuration with many edges having $\beta = 0$. Our simple strategy of setting these gradients to zero works quite well in this example. After a few steps all β angles have become sufficiently non-zero (above our threshold of $\varepsilon = 10^{-6}$) that the flow proceeds as expected.

Figure 11 shows an example of mesh restoration. A set of triangles is marked as free while all others are held fixed.
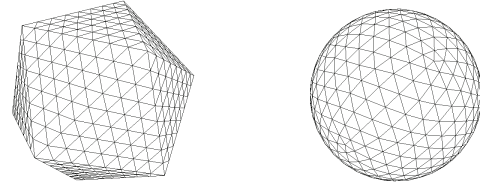
Figure 6: *Subdivided icosahedron rapidly evolves to a sphere.*
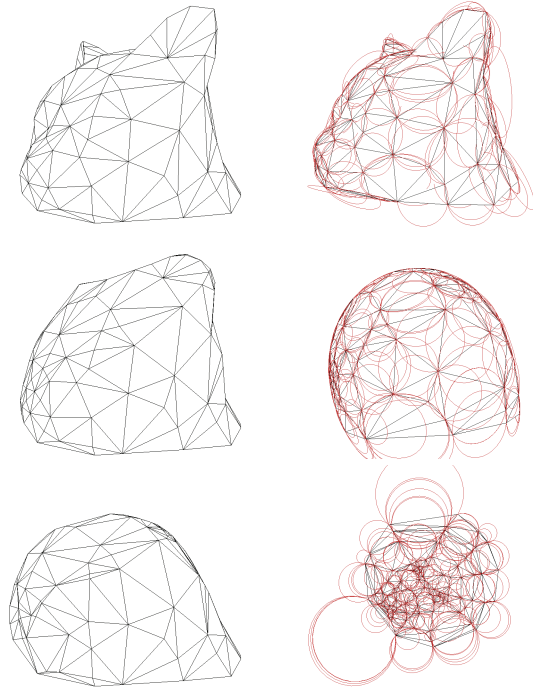

Figure 7: *Cathead evolved with fixed boundaries (left column) and free boundaries (right column). In each case the original mesh is followed by an intermediate state of the evolution and the final state.*

The free vertices flow to "repair" the scar with a surface section which smoothly (G^1) interpolates the surrounding fixed surface (compare to the example in [CDD*04]).

Finally Figure 12 shows an example of geometry denoising. The mesh smoothed in this case is the raw result of a light field scanner with typically small amplitude noise due to measurement error. In particular for examples of this type the non-shrinking nature of the Willmore flow (the energy is scale invariant) favors it over standard approaches based on mean curvature flow. The mesh contains over 37k vertices (and 88 boundary loops). This mesh is particularly challenging since it contains many edges with β near zero: the original mesh is a triangulated quadrangulation. It also has many triangles with very high aspect ratio right next to small, round triangles. Figure 12 shows the original mesh followed by the results of 10 respectively 100 smoothing steps.
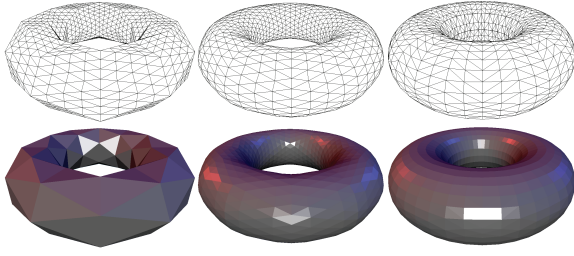
Figure 8: *A twice linearly subdivided torus mesh evolves quickly towards a geometric torus with long term flow changing the shapes of triangles so as to align edges with principal curvature directions.*
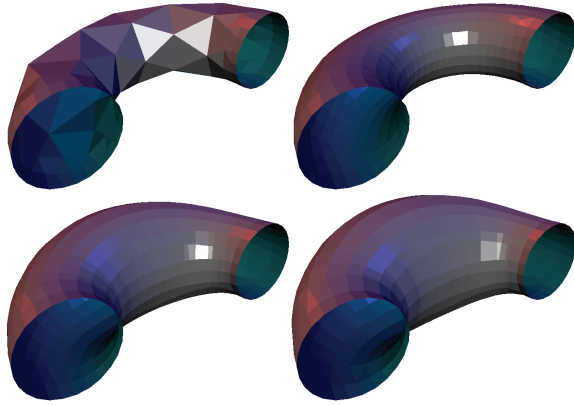

Figure 9: *Time evolution of a pipe with circular boundary conditions. Compare with Figure 8.*

5. Conclusion

In this paper we have considered a discrete Willmore flow. The discrete energy is expressed in terms of circles and the angles they make with one another and therefore Möbius invariant, reproducing the symmetries of the continous energy. The discrete energy approaches the continuous energy in the infinitesimal limit for regular triangulations with two edges aligned with principal curvature directions. We have experimented with a number of different linear and non-linear solvers and found a simple linear approximation of the Hessian to be sufficient in our experiments.

Ongoing investigations are geared towards more powerful numerical methods. Especially for large meshes a multi-grid solver for the linear systems arising in the semi-implicit time stepping method may well provide significant speedups over our current (unoptimized) implementation. Possible future directions include the use of Willmore gradient flow for the construction of variational subdivision schemes which would optimize functionals such as $\int \kappa_1{}^2 + \kappa_2{}^2 \, dA$ in a fully non-linear fashion. Another interesting avenue is the use of the Willmore functional to construct curvature line nets. We have observed that the discrete Willmore flow leads to
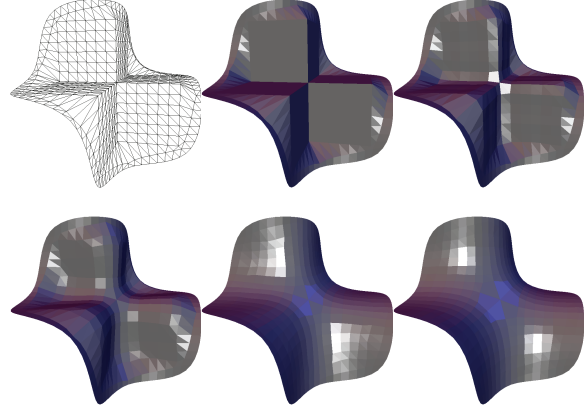

Figure 10: *Smooth filling of a six sided hole. On the upper left the original configuration showing the underlying mesh. The boundary triangles follow a smooth outline and fix position and tangency constraints (all other vertices are unconstrained). Evolution to the energy minimum is illustrated through a number of intermediate steps with the final hole fill in the lower right. All shaded images use triangle normals for shading without interpolation.*
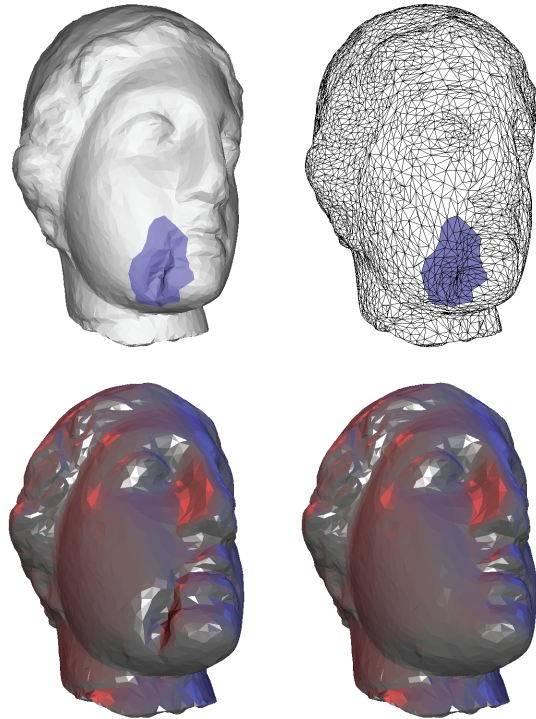

Figure 11: *Surface restoration for the Egea model. A region to be restored is outlined (top). All vertices in the blue triangles are unconstrained with the surrounding vertices providing position and tangency constraints. Results of the energy minimization (before and after; bottom).*
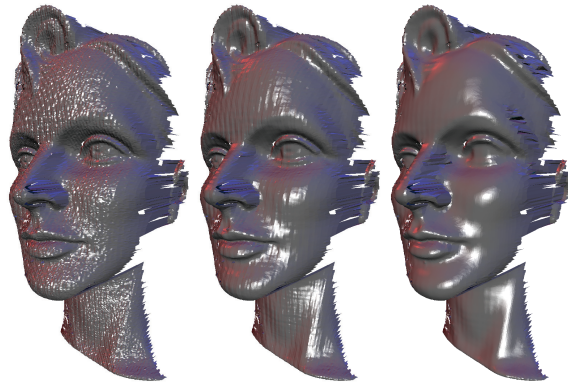
Figure 12: *Denoising of scanned geometry. On the left the original mesh with noise due to an active light stripe based scanner. Followed by the results of 10 and 100 smoothing steps (37k vertices; 88 boundary loops).*

meshes aligned with the curvature lines of the surface. This phenomenon, theoretically partially explained in Section 2, is quite natural since the curvature lines are also a subject of Möbius geometry. A closely related problem, currently under investigation, is the definition of the discrete Willmore energy for quadrilateral meshes, which in a sense would be more natural for curvature line nets.

References

[BBE*04] BALAY S., BUSCHELMAN K., EIJKHOUT V., GROPP W. D., KAUSHIK D., KNEPLEY M. G., MCINNES L. C., SMITH B. F., ZHANG H.: *PETSc Users Manual*. Tech. Rep. ANL-95/11 - Revision 2.1.5, Mathematics and Computer Science Division, Argonne National Laboratory, 2004. Available at http://www-unix.mcs.anl.gov/petsc/petsc-2/. 6

[Bla29] BLASCHKE W.: *Vorlesungen über Differentialgeometrie III*. Springer, 1929. 1, 2

[BMF03] BRIDSON R., MARINO S., FEDKIW R.: Simulation of clothing with folds and wrinkles. In *Proceedings of the 2003 ACM SIGGRAPH/Eurographics Symposium on Computer animation* (2003), Eurographics Association, pp. 28–36. 1

[BMMS04] BENSON S. J., MCINNES L. C., MORÉ J., SARICH J.: *TAO User Manual (Revision 1.7)*. Tech. Rep. ANL/MCS-TM-242, Mathematics and Computer Science Division, Argonne National Laboratory, 2004. Available at http://www-unix.mcs.anl.gov/tao. 6

[Bob05] BOBENKO A. I.: A Conformal Energy for Simplicial Surfaces. In *Combinatorial and Computational Geometry*, Goodman J. E., Pach J.,, Welzl E., (Eds.), MSRI Publications. Cambridge University Press, 2005, pp. 133–143. 2, 3, 4

[Can70] CANHAM P. B.: The Minimum Energy of Bending as a Possible Explanation of the Biconcave Shape of the Human Red Blood Cell. *Journal of Theoretical Biology 26* (1970), 61–81. 1

[CDD*04] CLARENZ U., DIEWALD U., DZIUK G., RUMPF M., RUSU R.: A Finite Element Method for Surface Restoration with Smooth Boundary Conditions. *Computer Aided Geometric Design 21*, 5 (2004), 427–445. 2, 7

[Che73] CHEN B.-Y.: An Invariant of Conformal Mappings. *Proceedings of the American Mathematical Society 40*, 2 (1973), 563–564. 2

[CS99] CHOPP D. L., SETHIAN J. A.: Motion by Intrinsic Laplacian of Curvature. *Interfaces and Free Boundaries 1*, 1 (1999), 107–123. 2

[DCDS97] DUCHAMP T., CERTAIN A., DEROSE T., STUETZLE W.: *Hierarchical Computation of PL Harmonic Embeddings*. Tech. rep., University of Washington, 1997. 2

[DDE03] DECKELNICK K., DZIUK G., ELLIOTT C. M.: Fully Discrete Semi-Implicit Second order Splitting for Anisotropic Surface Diffusion of Graphs. *SIAM J. Numer. Anal.* (2003). To appear. 2

[DMA02] DESBRUN M., MEYER M., ALLIEZ P.: Intrinsic Parameterizations of Surface Meshes. *Computer Graphics Forum (Proceedings of Eurographics 2002) 21*, 3 (2002), 209–218. 2, 5

[DMSB99] DESBRUN M., MEYER M., SCHRÖDER P., BARR A.: Implicit Fairing of Irregular Meshes using Diffusion and Curvature Flow. In *Computer Graphics (Proceedings of SIGGRAPH)* (1999), pp. 317–324. 2, 7

[DR04] DROSKE M., RUMPF M.: A Level Set Formulation for Willmore Flow. *Interfaces and Free Boundaries 6*, 3 (2004), 361–378. 2

[EDD*95] ECK M., DEROSE T. D., DUCHAMP T., HOPPE H., LOUNSBERY M., STUETZLE W.: Multiresolution Analysis of Arbitrary Meshes. In *Proceedings of SIGGRAPH* (1995), pp. 173–182. 2

[Fen29] FENCHEL W.: Über die Krümmung und Windung geschlossener Raumkurven. *Math. Ann. 101* (1929), 238–252. 3

[GHDS03] GRINSPUN E., HIRANI A., DESBRUN M., SCHRÖDER P.: Discrete Shells. In *Symposium on Computer Animation* (2003), pp. 62–67. 1

[GKS02] GRINSPUN E., KRYSL P., SCHRÖDER P.: CHARMS: A Simple Framework for Adaptive Simulation. *ACM Transactions on Graphics 21*, 3 (2002), 281–290. 1

[Gre94] GREINER G.: Variational Design and Fairing of Spline Surfaces. In *Proceedings of EUROGRAPHICS* (1994), vol. 13, pp. 143–154. 1

[GY03] GU X., YAU S.-T.: Global Conformal Surface Parameterization. In *Eurographics/ACM SIGGRAPH Symposium on Geometry Processing* (2003), pp. 127–137. 2

[Hel73] HELFRICH W.: Elastic Properties of Lipid Bilayers: Theory and Possible Experiments. *Zeitschrift für Naturforschung Teil C 28* (1973), 693–703. 1

[HES03] HAUTH M., ETZMUSS O., STRASSER W.: Analysis of numerical methods for the simulation of deformable models. *The Visual Computer 19*, 7–8 (2003), 581–600. 7

[HGR01] HARI L. P., GIVOLI D., RUBINSTEIN J.: Computation of Open Willmore-Type Surfaces. *Applied Numerical Mathematics 37* (2001), 257–269. 2

[LP88] LOTT N. J., PULLIN D. I.: Method for Fairing B-Spline Surfaces. *Computer-Aided Design 20*, 10 (1988), 597–600. 1

[May01] MAYER U. F.: Numerical Solution for the Surface Diffusion Flow in Three Space Dimensions. *Computational and Applied Mathematics 20*, 3 (2001), 361–379. 2

[Mer01] MERCAT C.: Discrete Riemann Surfaces and the Ising Model. *Communications in Mathematical Physics 218*, 1 (2001), 177–216. 2

[MS00] MAYER U. F., SIMONETT G.: Self-Intersections for the Surface Diffusion and the Volume Preserving Mean Curvature Flow. *Differential and Integral Equations 13* (2000), 1189–1199. 2

[PP93] PINKALL U., POLTHIER K.: Computing Discrete Minimal Surfaces and Their Conjugates. *Experimental Mathematics 2*, 1 (1993), 15–36. 2

[SK01] SCHNEIDER R., KOBBELT L.: Geometric Fairing of Irregular Meshes for Free-From Surface Design. *Computer Aided Geometric Design 18*, 4 (2001), 359–379. 2

[Spi75] SPIVAK M.: *A Comprehensive Introduction to Differential Geometry*, 3 ed. Publish or Perish, 1975. 3

[TWBO03] TASDIZEN T., WHITAKER R., BURCHARD P., OSHER S.: Geometric Surface Processing via Normal Maps. *ACM Transactions on Graphics 22*, 4 (2003), 1012–1033. 2

[Whi73] WHITE J. H.: A global invariant of conformal mappings in space. *Proceedings of the American Mathematical Society 38*, 1 (1973), 162–164. 2

[Wil00] WILLMORE T. J.: Surfaces in Conformal Geometry. *Annals of Global Analysis and Geometry 18*, 3-4 (2000), 255–264. 1

[WW94] WELCH W., WITKIN A.: Free-Form Shape Design Using Triangulated Surfaces. *Computer Graphics (Proceedings of SIGGRAPH) 28* (1994), 247–256. 1

[XPB05] XU G., PAN Q., BAJAJ C. L.: Discrete Surface Modeling using Geometric Flows. *Computer Aided Geometric Design* (2005). To appear. 2

[YB02] YOSHIZAWA S., BELYAEV A. G.: Fair Triangle Mesh Generation with Discrete Elastica. In *Geometric Modeling and Processing* (2002), IEEE Computer Society, pp. 119–123. 2